J. Fluid Mech. (1984), *vol.* 141, *pp.* 123–138
Printed in Great Britain

Behaviour of a converging-channel breakwater; theory and experiment

By D. I. PULLIN
Department of Mechanical Engineering, University of Queensland, St. Lucia Qld. 4067, Australia

AND P. N. JOUBERT
Department of Mechanical Engineering, University of Melbourne, Parkville, Vic. 3052, Australia

(Received 1 August 1983)

The energy-transmission characteristics of an array of open convergent-channel-type wavebreakers to a normally incident wavetrain is studied experimentally and theoretically. A model of the wavebreaker transmission response to a sinusoidal incident wavetrain on a constant-depth ocean is developed as a boundary-value problem within the framework of linearized water-wave theory. This results in an integral equation based on a Green-function solution to the Helmholtz equation, which is solved numerically for each of several wavebreaker geometries over a range of incident wavelengths. Experiments on fixed model wavebreakers performed in an open wave tank are described, and results are compared with the numerical predictions. Theory and experiment indicate that the convergent-channel design is effective in attenuating the transmitted wave at resonant values of the incident wavelength λ that scale on the channel length L. Forces experienced by each half-wavebreaker are largely transverse; the calculated longitudinal forces for the fixed breakwater are small compared to those on a solid wall except at one resonance near $L/\lambda = 0.5$. Experiments indicate that this last condition does not occur for a floating breakwater, where the corresponding transmission of wave energy is high.

1. Introduction

While observing the wave-diffraction pattern generated by a row of parallel moored yachts in a marina, one of us (PNJ) noticed that the sequence of convergent channels formed between the bows of adjacent boats appeared to attenuate an onshore incident wavetrain, even though there was finite separation of boat hulls. The waters on the leeside were relatively calm, indicating that the moored vessels were operating effectively as wavebreakers. The passage between adjacent boats first converged to the points of minimum vessel separation and then diverged to the sterns. It was observed that as incident waves reflected obliquely from the boat hulls their amplitudes first increased in the convergent section but thereafter diminished rapidly past the passage throat. The boats responded to the wave excitation through oscillation mainly in pitch and in roll.

In *Transportable Breakwaters – A Survey of Concepts* (1971) no fewer than 106 different types are listed, designed to operate on widely differing principles. These include both floating and energy-absorbing configurations in addition to several variations on the conventional rock-fill breakwater. None of the catalogued designs, however, appear to utilize the wave-attentuation properties of a converging channel.

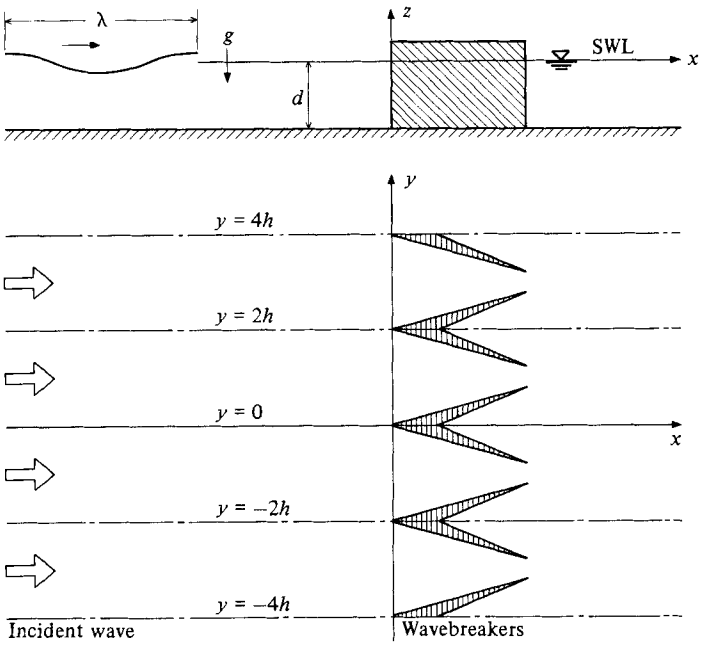

FIGURE 1. Progressive waves incident on wavebreaker array in water of constant depth d. Wavebreakers are symmetrical about $y = 2mh, m = -\infty, \ldots, -1, 0, 1, \ldots, \infty$.

A possible schematic design of a breakwater consisting of an array of vertical-sided channel-type wavebreakers is shown in figure 1. We suggest that this configuration may offer several advantages over more-conventional types. The open structure allows mass transfer and will permit waves of both very small (ripples) and large wavelength to pass through largely unattenuated, so that the breakwater will operate as a high- and low-pass filter. The interaction of the reflected part of the spectrum of incident wavelengths with the wavebreaker array will take place largely in the gently narrowing channel openings, thus reducing wave-breaking and slamming forces often experienced by breakwater surfaces parallel to incident wavecrests. Subsequently the forces experienced by the wavebreaker will be largely transverse with the component in the direction of the incident wave distributed over the large surface area of the channel walls. This may be of particular importance for reduction of mooring forces in a floating configuration.

The aim of the present study is thus to investigate theoretically and experimentally the performance of an open-channel wavebreaker. We consider a simplified model in which each component of the array consists of two vertical plates or wedges arranged in a V-shape and fixed to the ocean floor. In §2 an integral equation is obtained for the solution of the Helmholtz equation describing the diffracted wave pattern produced by the wavebreaker array. A scheme for the numerical solution of this equation is given in §2.3. The present experiments are described in §3 and comparison between the experiments and theory are discussed in §4. Although we are presently concerned with the fixed breakwater, the possible relevance of the present results to the more difficult (and interesting) floating-array configuration is discussed briefly in §5.

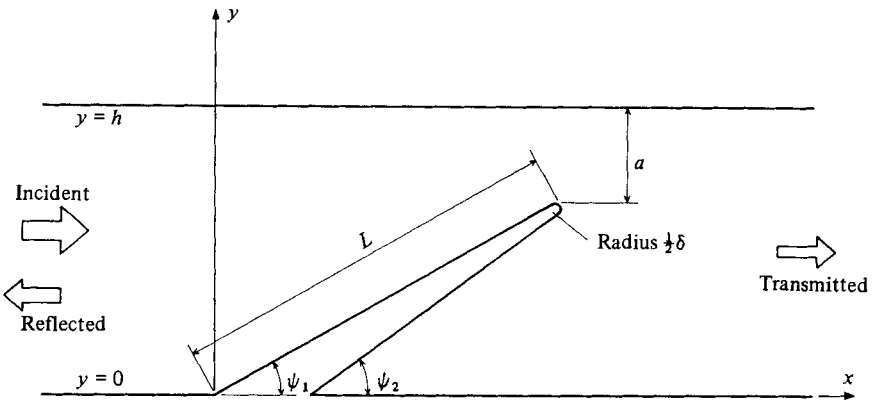

FIGURE 2. Flow in strip $h \geqslant y \geqslant 0$ showing geometry of half-wavebreaker.

2. Theory

2.1. *Statement of problem*

We consider the interaction of a field of incident progressive waves on an inviscid ocean of constant depth d with an infinite array of identical wavebreakers. The basic configuration is as shown in figure 1. The Cartesian (x, y, z) coordinate system is such that the positive x-axis lies in the direction of motion of the incident waves, which are normally incident on the array and of wavelength λ. Gravity g acts in the negative z-direction. The solid fixed wavebreakers extend to the ocean floor and are two-dimensional in (x, y) cross-section. Each wavebreaker must be symmetrical about its centreline at $y = 2mh$, $m = -\infty, \ldots, 0, \ldots, +\infty$, but its shape is otherwise arbitrary. Owing to this overall symmetry of the wave–wavebreaker system we may restrict attention to the equivalent case of flow in a strip or half-channel in $h \geqslant y \geqslant 0$ with solid walls on $y = 0$ and $y = h$ as shown in figure 2.

We note here that the assumption of normally incident waves is a significant simplification, since in practice waves will be obliquely incident. We believe that the Green-function approach given in §2.2 may be extended to the case of general incidence, but owing to symmetry breaking the computational effort required for the present wavebreaker geometry is substantially increased. The effects – possibly quite profound – of wave incidence are thus left for future investigation.

The irrotational fluid motion is described by a velocity potential Φ satisfying

$$\frac{\partial^2 \Phi}{\partial x^2} + \frac{\partial^2 \Phi}{\partial y^2} + \frac{\partial^2 \Phi}{\partial z^2} = 0. \tag{1}$$

We seek a solution to (1) in the form

$$\Phi(x, y, z, t) = \frac{a_{\mathrm{I}} g \cosh\left[k(z+d)\right]}{\mathrm{i}\omega \cosh\left(kd\right)} \mathrm{e}^{-\mathrm{i}\omega t} \phi(x, y), \tag{2}$$

where ω is the frequency, a_{I} and k are real constants and $\phi(x, y)$ is a complex-valued function. In (2), and elsewhere here, physical quantities will be understood to be the real part of generally complex functions. Substituting (2) into (1) gives the two-dimensional Helmholtz equation for ϕ:

$$\frac{\partial^2 \phi}{\partial x^2} + \frac{\partial^2 \phi}{\partial y^2} + k^2 \phi = 0. \tag{3}$$

The height of the ocean free surface above the still-water line $z = 0$ is $z = \eta(x, y, t)$. We assume that amplitudes of the free surface are everwhere small, so that ϕ and η satisfy the linearized free-surface kinematic and dynamic conditions respectively as

$$\left.\begin{aligned} \frac{\partial \Phi}{\partial z} - \frac{\partial \eta}{\partial t} &= 0, \\ \frac{\partial \Phi}{\partial t} + g\eta &= 0 \end{aligned}\right\} \quad \text{on} \quad z = 0. \tag{4}$$

Substituting (2) into (4) gives

$$\eta(x, y, t) = a_1 \phi(x, y)\, \mathrm{e}^{-\mathrm{i}\omega t}, \tag{5}$$

$$\omega^2 = gk \tanh(kd). \tag{6}$$

Letting the incident plane wave from $x = -\infty$ be given by

$$\phi_{\mathrm{I}} = \mathrm{e}^{\mathrm{i}kx}, \tag{7}$$

(5) shows that we may put $k = 2\pi/\lambda$, where λ is the incident wavelength while (6) is the linearized dispersion relationship and $a_{\mathrm{I}} \ll \lambda$ is the incident wave amplitude. Note that the use of (4) means that we cannot describe nonlinear phenomena such as wavebreaking.

The scattering problem is now to find $\phi(x, y)$ satisfying (1) and the zero-normal-velocity boundary condition given, from (2), by

$$\frac{\partial \phi}{\partial n} = 0, \tag{8}$$

on $y = 0$, $y = +h$ and on $\mathscr{C}$, the shape of the half-wavebreaker in the (x, y)-plane in figure 2, $\boldsymbol{n}$ being the outward normal. Putting

$$\phi(x, y) = \phi_{\mathrm{I}} + \phi_{\mathrm{S}}, \tag{9}$$

where ϕ_{S} represents the wave scattered by the wavebreaker, the radiation condition requires that ϕ_{S} represents an outgoing wave as $|x| \to \infty$. The asymptotic form of ϕ_{S} for large $|x|$ cannot be specified *a priori*, and will be discussed subsequently.

2.2. *Integral-equation formulation*

In the remainder of §2, except where otherwise specified, all quantities will be assumed to be in non-dimensional form with length- and timescales h and $(h/g)^{\frac{1}{2}}$ respectively. Applying Green's identity to ϕ_{S}, we obtain the well-known result (Morse & Feshbach 1953)

$$\mu \phi_{\mathrm{S}}(\boldsymbol{r}) = \frac{1}{4\pi} \int_S \left[G(\boldsymbol{r}|\boldsymbol{r}') \frac{\partial \phi_{\mathrm{S}}'}{\partial n'} - \phi_{\mathrm{S}}' \frac{\partial G(\boldsymbol{r}|\boldsymbol{r}')}{\partial n'} \right] \mathrm{d}s'. \tag{10}$$

In (10) S refers to a closed contour formed of $\mathscr{C}$, the lines $y = 0$ and $y = 1$ and closed by lines $x =$ constant denoted by $X_{-\infty}$ and X_{∞} at $x \to \pm\infty$. The Green function $G(\boldsymbol{r}|\boldsymbol{r}')$ is a fundamental solution to (3), with $\boldsymbol{r}$ being a general point and $\boldsymbol{r}'$ a point on S. Dashed quantities are those evaluated on S, and $\mu = 1$ if $\boldsymbol{r}$ lies inside S, $\mu = \frac{1}{2}$ if $\boldsymbol{r}$ lies on S (but not at a corner) and $\mu = 0$ otherwise. On S, s' is the arclength.

We now choose $G(\boldsymbol{r}|\boldsymbol{r}')$ in the form

$$G(\boldsymbol{r}|\boldsymbol{r}') = \pi\mathrm{i} \sum_{\nu=-\infty}^{\infty} [H_0^{(1)}(k((x-x')^2 + (y-y'-2\nu)^2)^{\frac{1}{2}}) + H_0^{(1)}(k((x-x')^2 + (y+y'-2\nu)^2)^{\frac{1}{2}})], \tag{11}$$

where $H_0^{(1)}(kr)$ is the Hankel function of the first kind and zeroth order, which is the well-known radiating-source fundamental solution of (3). Equation (11) is the solution of (3) at $\boldsymbol{r} = (x, y)$ due to a unit source at $\boldsymbol{r}' = (x', y')$ on $\mathscr{C}$ together with two infinite arrays of image sources at the points $(x', y'+2\nu)$, $\nu = -\infty, \ldots, -1, 1, \ldots, \infty$ and $(x', -y'+2\nu)$, $\nu = -\infty, \ldots, +\infty$. The image system is constructed such that

$$\left[\frac{\partial G(\boldsymbol{r}|\boldsymbol{r}')}{\partial y'}\right]_{y=0,\ y=1} = 0, \tag{12}$$

which follows from

$$(\partial G/\partial y)_{y=0,\ y=1} = 0$$

and the reciprocity relation

$$G(\boldsymbol{r}|\boldsymbol{r}') = G(\boldsymbol{r}|\boldsymbol{r}).$$

Equations (7) and (9) show that $\partial\phi_S/\partial y = 0$ on $y = 0$ and 1, and this result together with (12) shows that the contribution to the integral in (10) from that part of S on $y = 0$, $y = 1$ must vanish. Since in (10), (11) we have utilized only the radiating-unit-source solution, it follows that ϕ_S must represent an outward-going wave as $|x| \to \infty$. Hence the overall solution (9) must satisfy the radiation condition for large $|x|$, from which it follows that the contribution to (10) from X_∞ and $X_{-\infty}$ must vanish (this can be verified subsequently). Using (7)–(9), (10) then becomes

$$\mu\phi_S(r) = -\frac{1}{4\pi}\int_{\mathscr{C}}\left[G(\boldsymbol{r}|\boldsymbol{r}')\frac{\partial}{\partial n'}(e^{ikx'}) + \phi_S'\frac{\partial G(\boldsymbol{r}|\boldsymbol{r}')}{\partial n'}\right]ds', \tag{13}$$

Letting $\boldsymbol{r} \to$ a point on $\mathscr{C}$ gives $\mu = \frac{1}{2}$, and (13) becomes a Fredholm integral equation of the second kind for ϕ_S on $\mathscr{C}$. The numerical solution of (13) and (11) is the basis for the present calculations.

Equation (11) is not a convenient form of G for either numerical or asymptotic evaluation. Alternative equivalent expressions are given by Morse & Feshbach (1953) as

$$G(\boldsymbol{r}|\boldsymbol{r}') = 2\pi i \sum_{\nu=0}^{\infty} \epsilon_\nu \cos(\pi\nu y)\cos(\pi\nu y')\frac{e^{iQ_\nu|x-x'|}}{Q_\nu}, \tag{14a}$$

where $\epsilon_0 = 1$, $\epsilon_\nu = 2$, $\nu \geqslant 1$, and

$$G(\boldsymbol{r}|\boldsymbol{r}') = R(y+y'|x-x') + R(y-y'|x-x') + \frac{2\pi i}{k}e^{ik|x-x'|} + 4\sum_{\nu=1}^{\infty}\cos(\pi\nu y')\cos(\pi\nu y)\left[\frac{i\pi e^{iQ_\nu|x-x'|}}{Q_\nu} - \frac{e^{-\pi\nu|x-x'|}}{\nu}\right]. \tag{14b}$$

In (14*a*, *b*)

$$R(Y|X) = -\ln[1 - 2e^{-\pi|X|}\cos(\pi Y) + e^{-2\pi|X|}], \tag{14c}$$

$$Q_\nu = (k^2 - \pi^2\nu^2)^{\frac{1}{2}} = iR_\nu, \quad R_\nu = (\pi^2\nu^2 - k^2)^{\frac{1}{2}} \quad (\pi\nu > k), \tag{14d}$$

and the branch of the square root has been chosen so that $G(\boldsymbol{r}|\boldsymbol{r}')$ gives *outgoing* waves as $|x| \to \infty$.

Use of (14*a*) in (13) then leads to the modal expansion for the transmitted ($x > L\cos\psi_1$) and reflected waves ($x < 0$) respectively:

$$\phi_{\pm S} = \sum_{\nu=0}^{P} D_{\pm\nu}\cos(\pi\nu y)e^{\pm iQ_\nu x} + \sum_{\nu=P+1}^{\infty} D_{\pm\nu}\cos(\pi\nu y)e^{-R_\nu|x|}, \tag{15a}$$

where P is the smallest integer satisfying $(P+1)\pi > k$, and for $P \leqslant \nu$

$$\left.\begin{aligned} D_{+\nu} &= \tfrac{1}{2}\epsilon_\nu \int_{\mathscr{C}} e^{-iQ_\nu x'}\left[\sin\theta' \cos(\pi\nu y')\left(\frac{k\,e^{ikx'}}{Q_\nu} - \phi_S'\right) - i\phi_S' \frac{\pi\nu \cos\theta' \sin(\pi\nu y')}{Q_\nu}\right] ds', \\ D_{-\nu} &= \tfrac{1}{2}\epsilon_\nu \int_{\mathscr{C}} e^{iQ_\nu x'}\left[\sin\theta' \cos(\pi\nu y')\left(\frac{k\,e^{ikx'}}{Q_\nu} + \phi_S'\right) - i\phi_S' \frac{\pi\nu \cos\theta' \sin(\pi\nu y')}{Q_\nu}\right] ds', \end{aligned}\right\} \quad (15b)$$

where θ' is the local tangent angle to $\mathscr{C}$. As $x \to \pm\infty$ each term of the second series in (15a) decays exponentially, so that asymptotically the scattered wave is a system of $P+1$ outgoing components. The zeroth order ($\nu = 0$) is a plane wave of wavenumber $(k_x, k_y) = (\pm k, 0)$ corresponding to the incident mode. The higher-order modes ($P \geqslant \nu \geqslant 1$) represent oblique, multiply reflecting wave systems with wavenumber components $(Q_\nu, \pm\pi\nu)$, $x \to +\infty$, and $(-Q_\nu, \pm\pi\nu)$, $x \to -\infty$, $\nu = 1, \ldots, P$, generated by image-interference effects. For $k = p\pi, p = 1, 2, \ldots$, (14) contains square-root singularities corresponding to transverse resonance effects (Ursell 1951), where the representation (13), (14) fails. Use of (14a) and (15) in (10) shows that the contribution to the integral from $X_{-\infty}$ and X_∞ indeed vanishes. Note that (15) agrees with results obtained by Srokosz (1980) using a different method.

The incoming and outgoing time-averaged flux of energy across $X_{-\infty}$ and X_∞ must be in balance, since, first, the wavebreaker does not extract energy, and, secondly, we have neglected viscous dissipation. This leads to a relationship between the $D_{+\nu}, D_{-\nu}$ which may be obtained by applying Green's theorem to ϕ and its complex conjugate ϕ^* (Newman 1976). Use of (7)–(9) and (15) then yields

$$|D_{-0}|^2 + |1 + D_{+0}|^2 + \frac{1}{(2k)} \sum_{\nu=1}^{P} Q_\nu (|D_{-\nu}|^2 + |D_{+\nu}|^2) = 1, \quad (16)$$

expressing time-averaged energy conservation.

Since the present experiments were limited to dimensional wavelengths greater than $2h$ in figure 1, we restrict attention in the calculations subsequently described to waves with $\lambda > 2$. Hence $P = 0$ in (15a), and the scattered wave contains only the plane fundamental mode. We note, however, that the present method is able to handle $\lambda < 2$, except near the irregular wavelengths $k = p\pi$, where special solution methods are required (for a discussion see Mei 1978). Once ϕ_S on $\mathscr{C}$ is known, D_{+0} and D_{-0} can be calculated from (15c). The transmitted and reflected complex free-surface amplitudes are

$$a_T = a_I(1 + D_{+0}), \quad a_R = a_I D_{-0}. \quad (17)$$

The fraction of the incident energy transmitted is $E_T = |1 + D_{+0}|^2$. The fraction reflected is $E_R = |D_{-0}|^2$, and energy conservation becomes simply

$$E_T + E_R = 1. \quad (18)$$

The dimensional force exerted by the fluid on each half-wavebreaker is

$$\{F_x, F_y\} = \int_{-d}^{0} \int_{\mathscr{C}} p' \{\sin\theta', -\cos\theta'\}\, ds'\, dz, \quad (19)$$

where the pressure p is given by $p = -\rho\, \mathrm{Re}\{\partial\Phi/\partial t\}$, ρ being the water density. Using (2) we obtain

$$\frac{2\pi\{F_x, F_y\}}{\rho g a_I \lambda h^2 \tanh(2\pi d/\lambda)} = \mathrm{Re}\left[e^{-i\omega t} \int_{\mathscr{C}} (\phi_S' + e^{ikx'}) \{\sin\theta', -\cos\theta'\}\, ds'\right]. \quad (20)$$

2.3. *Numerical solution*

We use an approximate numerical method to solve (13) ($\mu = \frac{1}{2}$) and (11). First $\mathscr{C}$ is divided into an adequately large number N of straight-line segments of length $\Delta s_n = s_n - s_{n-1}$, $n = 1, \ldots, N$, with midpoints $\bar{r}_n = (\bar{x}_n, \bar{y}_n)$. It is assumed that $\phi_S = \phi_S^{(n)}$ is constant over the nth segment and likewise that $e^{ikx'}$ in the integral in (13) is constant and given by $e^{ik\bar{x}_n}$ over the segment. A discretized form of the integral equation is then obtained by satisfying it at $\bar{r}_n$, $n = 1, \ldots, N$. This results in N complex linear equations for the $\phi_S^{(n)}$ which we write as

$$\tfrac{1}{2}\phi_S^{(n)} + \frac{1}{4\pi}\sum_{j=1}^{N} \phi_S^{(j)} A_{nj} = -\frac{ik}{4\pi}\sum_{j=1}^{N} \sin\theta_j \, e^{ik\bar{x}_j} B_{nj} \quad (n = 1, \ldots, N), \tag{21a}$$

where

$$A_{nj} = \int_{s_{j-1}}^{s_j} \frac{\partial G(\bar{r}_n | r')}{\partial n'} \, ds', \tag{21b}$$

$$B_{nj} = \int_{s_{j-1}}^{s_j} G(\bar{r}_n | r') \, ds'. \tag{21c}$$

Equations (21 *a*) may be solved by a standard method once the integrals (21 *b*, *c*) are evaluated. The kernels in (21) were calculated from (14 *b*, *c*) and their derivatives. The rapidly convergent series terms were evaluated as double-precision (64 bit) sums to order M, where $|\exp(-\pi(M^2 - (k/\pi)^2)^{\frac{1}{2}}|x - x'|)|$ was of the order of single-precision (32 bit) accuracy. The residual sum in $(M+1, \ldots, \infty)$ was then obtained by a simple integral approximation.

For small $R = |r - r'|$ it may be shown that

$$G(r|r') = (-1 + \tfrac{1}{2}k^2R^2)\ln R^2 + F(r|r'), \tag{22}$$

where $F(R) \in C^3$ at $R = 0$. Putting $R_{jn} = |r_j - r_n|$, where r_j is a point on segment j, A_{nj} and B_{nj} were calculated by first splitting G and $\partial G/\partial n'$ according to (22). The component integrals of the $\ln R^2$ term were then evaluated analytically in each segment, taking due care near the $\ln R$ and R^{-1} Cauchy principal-value singularities in B_{nn} and A_{nn} respectively. The integrals of $F(r|r')$ were approximated with a three-point Simpson rule over the segment. For segments close to the image lines $y = 0, 1$, the contributions due to nearby image elements were isolated and also treated by singularity extraction.

The only satisfactory means of testing solution accuracy in practice is to demonstrate convergence with increasing N. A further check on global accuracy (but by no means a complete check) is given by the error in satisfying (18). For a test on a circular-cylinder wavebreaker of unit radius, the calculated a_R and a_T were found to be independent of N for $N \gtrsim 25$ with $\Delta s \approx \pi/N$. Excellent results satisfying (18) to within 0.005 were obtained for $N = 30$ over a broad range of k.

The half-wavebreaker geometry considered presently is illustrated in figure 2. It consists of two plane surfaces at angles ψ_1 and ψ_2 joined smoothly by the arc of a circle of dimensional diameter $\delta = 0.08h$. The gap between the wavebreaker and $y = h$ is a and L is the length. With $\psi_1 = \psi_2$, the plate geometry actually tested is obtained, and this proved to be a rather difficult case to calculate accurately. The reason is that for $\delta = 0$ the representation given in (10) becomes degenerate and the correct formulation is then in terms of dipoles only. This leads to a model which is quite unsuited to numerical treatment, since the resulting integral equation is of the first kind and moreover it contains a rather more complicated kernel than those in (13).

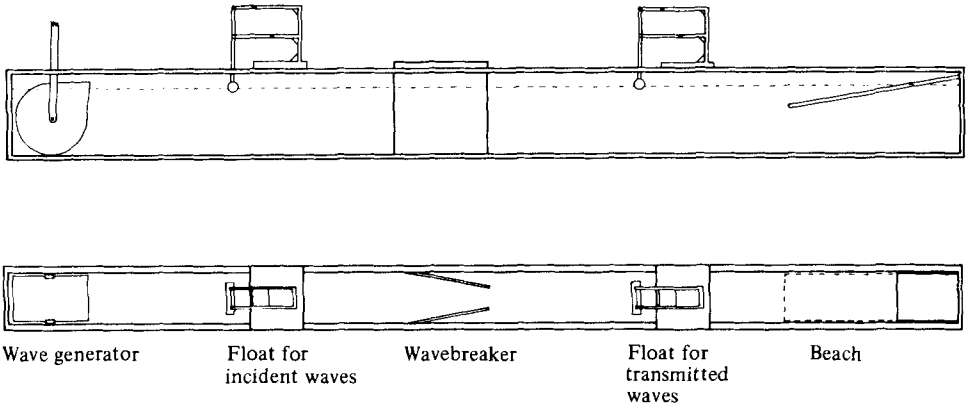

FIGURE 3. Wave tank and apparatus for wavebreaker experiments.

It was found, however, that, for small but finite δ, satisfactory results could be achieved using the present method with $\Delta s \approx \delta$. With $\Delta s = O(2L/N)$ this requires $N \sim 25(L/h)$ with $\delta = 0.08h$. The results for $L/h = 2.667$ ($L = 0.4$ m) with $N = 70$ in figures 4–6 and for $L/h = 5.333$ ($L = 0.8$ m) with $N = 130$ in figures 7–8 satisfied (18) to within 0.1–0.5%. Some cases for $L/h = 2.667$, $a/h = 0.133$ were calculated with $N = 130$, and these showed three-figure agreement for a_T, a_R compared to the $N = 70$ results. For a long wavebreaker, $L/h = 8$ ($L = 1.2$ m), the results for a limited λ-range shown in figure 9 are a compromise value of $N = 150$ (execution time varies as N^3 for larger N) for which (18) was satisfied to within 1.5%. In all geometries equal Δs was used on both wavebreaker surfaces with 4 equally spaced points distributed on a circular arc.

3. Experiment

3.1. *Apparatus*

The experiments were conducted in a wave tank in the Department of Mechanical Engineering, University of Melbourne. The tank is constructed of glass and steel. It is 14.6 m long, 0.3 m wide and contains water of nominal depth 0.5 m. A schematic diagram of the apparatus is shown in figure 3. The wave generator was of the 'Salter-duck' type, which generates approximately sinusoidal progressive waves by an oscillatory pitching motion. The frequency and amplitude of the pitching motion could be controlled independently, giving independent control of the wavelength over the range 0.48–4 m and of the wave amplitude from near zero to about 6 cm. At the end of the tank an artificial beach was installed consisting of oblique layers of gauze and perspex plates perforated with a matrix of holes. The function of the beach was to absorb the incoming waves by turbulent dissipation of the incident energy so as to inhibit back-reflection effects.

Wave amplitudes in the tank were measured by means of floats, designed to operate as linear transducers for small wave amplitudes. A linear variable-difference transformer (LVDT) was fixed to each float, producing an output voltage which for small amplitudes is directly proportional to the vertical displacement of the float from its mean level. Output signals from the LVDTs were fed into a two-channel oscillographic recorder, enabling permanent records to be made of incident and transmitted

waveforms. The floats were calibrated by plotting output voltage against the measured change in mean level obtained by slowly filling and draining the tank. Thus the floats are assumed to operate quasi-statically.

The wavebreaker models tested consisted of rectangular perspex and/or wooden plates (hence $\psi_1 = \psi_2$ in figure 2) of thickness $\delta = 12$ mm and of lengths $L = 0.4$, 0.8 and 1.2 m. For a given L, the configuration utilized was that of two half-wavebreakers (i.e. 2 plates) positioned symmetrically with a central gap as shown in figure 3, such that the vertical tank walls acted (apart from viscous effects) as planes of symmetry separated by $2h = 30$ cm. Each model extended to the tank bottom and was held in position by a system of clamps, wooden blocks and rubber wedges.

3.2. *Procedure*

While the beach at one end of the tank was effective in absorbing transmitted waves, there proved to be no effective means of eliminating secondary reflection of the reflected waves at the wave generator leading to subsequent interference with the incident wavetrain. Thus the experiments could not be conducted in a quasi-steady state over long periods. The procedure adopted was thus to obtain measurements from a wavetrain containing a finite group of waves. The wave generator was turned on for a predetermined period so as to produce a group of waves long enough for incident and transmitted amplitudes to be measured but not so long as to produce secondary-reflection problems. The recorded waveforms were then closely examined to ensure that a quasi-steady state had been reached in each case. The transmitted waveform was observed to become substantially two-dimensional within 1.5 m downstream of the breakwater trailing edge, enabling a good measurement of its amplitude in this position. The incident waveform amplitude was set nominally from the previously calibrated wavegenerator amplitude control, but actual measurements were obtained from a float about 1 m downstream of the wavegenerator. Wavefrequencies were obtained directly from the accurately known wavegenerator frequency and corresponding wavelengths were obtained from (6). This simple method was tested (with no wavebreaker present) by moving one float relative to another so as to reduce the phase difference between their motions to zero. The floats must then be separated by an integral multiple of λ. Measured results agreed with (6) to within a few percent.

4. Results and discussion

As might be expected from the well-known analogy between acoustics and linearized water-wave theory, the general trend of the computed transmission response in figures 4–9 is qualitatively similar to the acoustical response of an area restriction in a duct (see Kinsler & Frey 1962). For increasing λ/h, a sequence of alternate resonances (defined here as an E_T minimum) and transmission maxima is followed by full transmission in the long-wavelength limit. At resonance $E_T = 0$ for all a/h considered, and the corresponding λ/h appear to be independent of a/h. In contrast the E_T maxima are approximately proportional to a/h over the calculated range. For $a/h > 0.6$ (not shown) this behaviour reversed with $E_T = 1$ at 'anti-resonance' independent of a/h. Zero transmission through finite gaps is well known and may occur in fully open channels with side (i.e. Helmholtz) resonators (Buchwald & Williams 1975).

Figures 4–9 indicate that resonant values of L/λ occur approximately in half-integral increments. This suggests that the mechanism of resonance is the establishment of a near-standing wave of $\frac{1}{2}, 1, 1\frac{1}{2}, 2, \ldots$ wavelengths in the converging channel formed

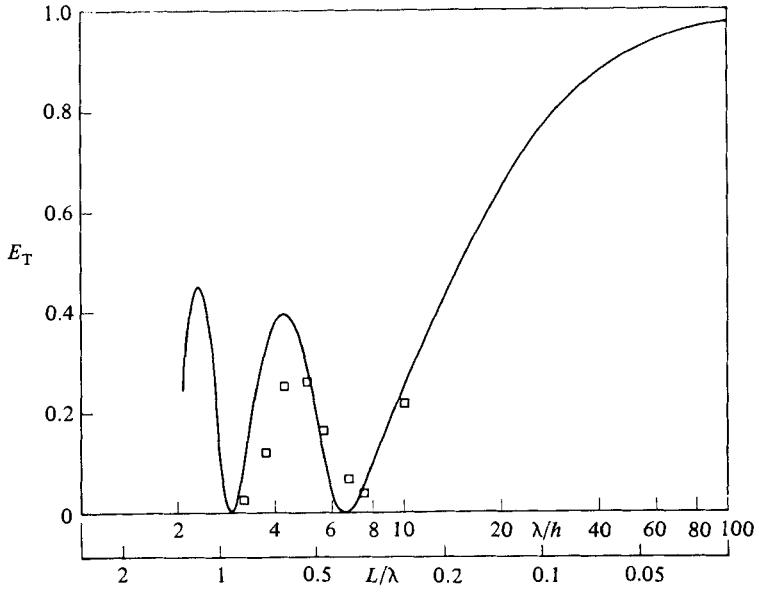

FIGURE 4. Energy-transmission response of flat-plate wavebreaker array; $L/h = 2.667$, $a/h = 0.133$, $\delta/h = 0.08$: ——, calculation; □, experiment.

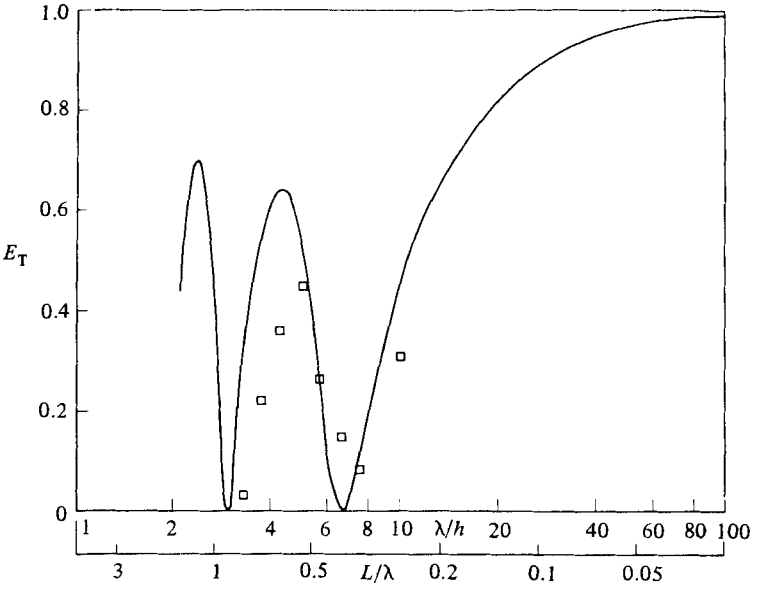

FIGURE 5. Energy-transmission response of flat-plate wavebreaker array; $L/h = 2.667$, $a/h = 0.2667$, $\delta/h = 0.08$: ——, calculation; □, experiment.

by the upstream wavebreaker surfaces. This is consistent with the amplitude-response characteristics for $L/h = 2.667$ shown at the minimum L/λ resonance in figure 10 and also with quarter-period wavebreaker wetted-surface profiles at two resonant conditions depicted in figure 11. Thus each channel operates somewhat like an acoustical horn, trapping the incident wave at resonance while radiating a strongly

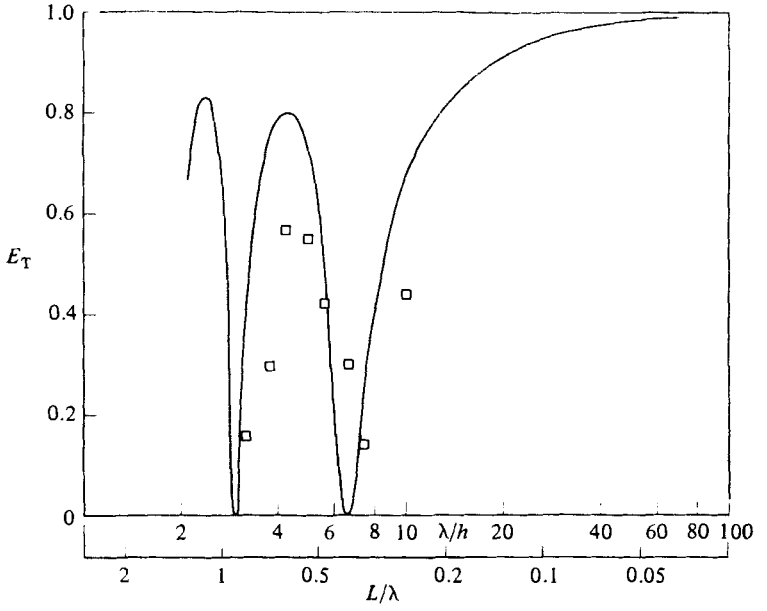

FIGURE 6. Energy-transmission response of flat-plate wavebreaker array; $L/h = 2.667$, $a/h = 0.40$, $\delta/h = 0.08$: ——, calculation; □, experiment.

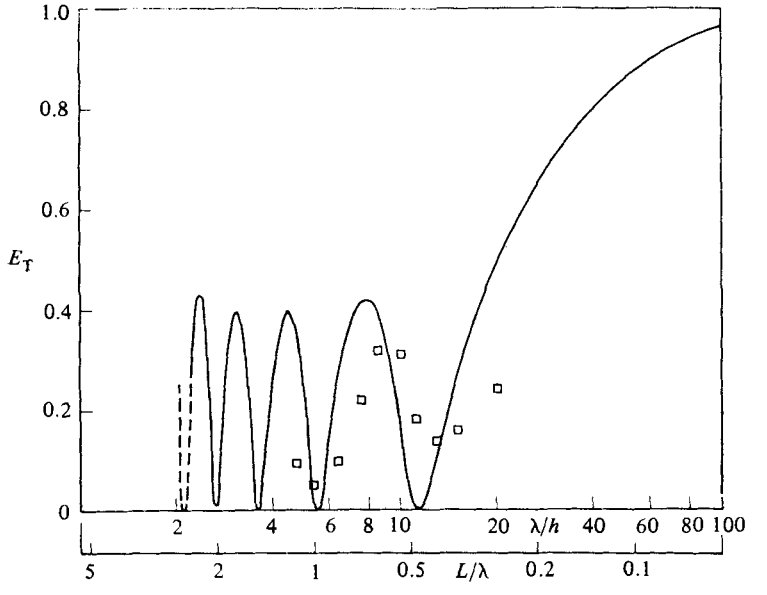

FIGURE 7. Energy-transmission response of flat-plate wavebreaker array; $L/h = 5.333$, $a/h = 0.133$, $\delta/h = 0.08$: ——, calculation; □, experiment.

directional (i.e. upstream) signal with negligible transmission. Additional phase information (not shown) indicated that at resonance the wave system between the converging channel walls is nearly planar, but is strongly three-dimensional in the immediate vicinity of the gap. In figure 10 the local amplitude $|\eta/a_T|$ is substantial in the region behind the wavebreaker, indicating strong interaction across the gap at resonance.

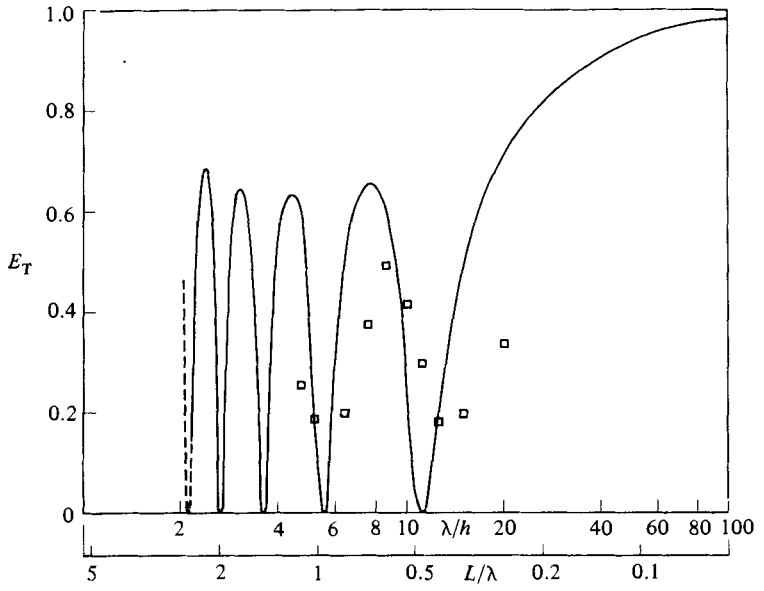

FIGURE 8. Energy-transmission response of flat-plate wavebreaker array; $L/h = 5.333$, $a/h = 0.267$, $\delta/h = 0.08$: ——, calculation; □, experiment.

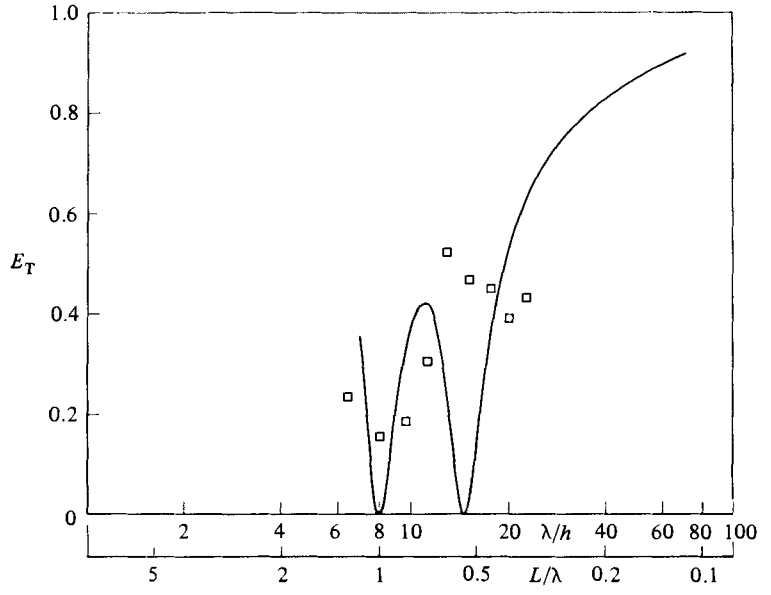

FIGURE 9. Energy-transmission response of flat-plate wavebreaker array; $L/h = 8.0$, $a/h = 0.133$, $\delta/h = 0.08$: ——, calculation; □, experiment.

The measured E_T shows general agreement with the calculations in figures 4–9 near the maximum resonant λ, but there is finite transmission as resonance and the measured E_T maxima are substantially less than the predictions. Apart from some viscous dissipation at the wavebreaker and tank boundaries, there are two principal sources of error not accounted for in the theory which will contribute to these

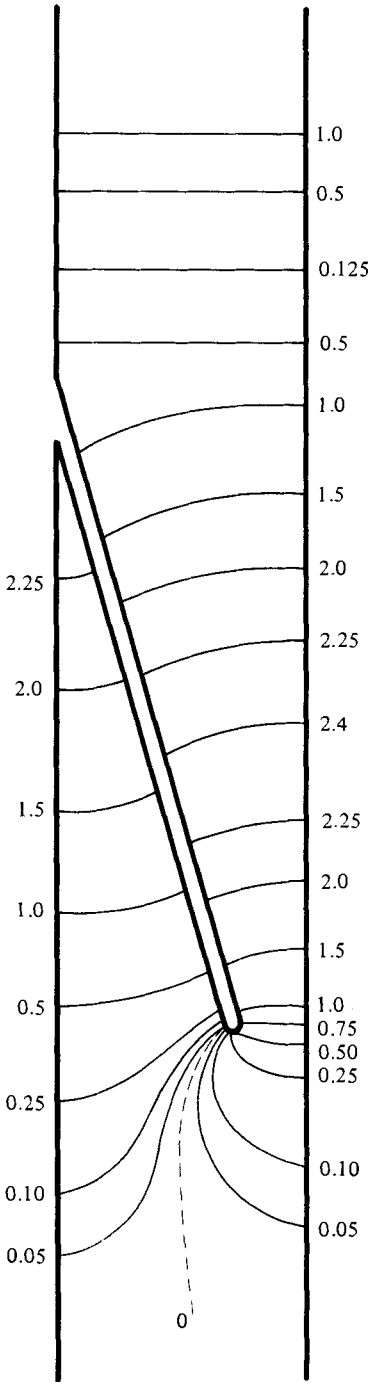

FIGURE 10. Contours of equal surface elevation amplitude; $L/h = 2.667$, $a/h = 0.267$, $\delta/h = 0.08$, $\lambda/h = 6.7$ (resonance). Values of $|\eta/a_1|$ as shown.

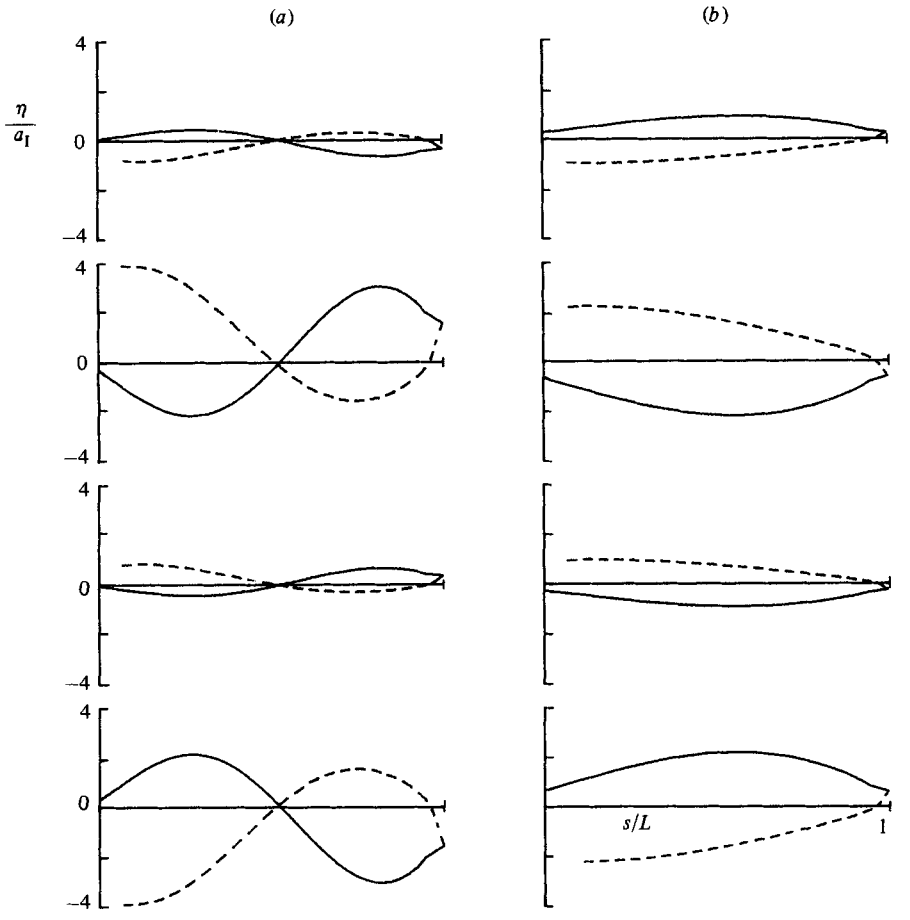

FIGURE 11. Wetted-surface profiles on wavebreaker at $\frac{1}{4}$ period intervals; $L/h = 2.667$, $a/h = 0.2667$: ——, upstream face; – – –, downstream face. Resonance conditions: (*a*) $L/\lambda = 0.90$; (*b*) $L/\lambda = 0.40$.

discrepancies. First there is the effect of finite wave amplitude. Incident wave amplitudes were of order 1–5 cm with maximum values of amplitude/λ well below the Stokes limit. Both theory and experiment however indicated large wave slope around the wavebreaker trailing edge for the range of incident amplitudes. While no large-scale wavebreaking or wave slamming against the wavebreaker surface was observed, some smaller-scale surface turbulence was noted near the exit gap. This may have been due to the presence of higher harmonics in the incident wavetrain which would be scattered quite differently to the fundamental frequency and may lead to an overestimate of $|a_1|$ and hence of the incident energy carried by the fundamental frequency. Secondly the co-oscillation (see figure 11) of fluid in the wedge sections on either side of the plate barrier at resonance will result in large velocities at the training edge. In fact, for $\delta \to 0, \psi_1 = \psi_2$ there will generally be a square-root singularity in the velocity. Thus we would expect the theoretical model to break down at the plate edge owing to flow separation resulting in oscillatory vortex formation.

The effect of varying ψ_2 while holding ψ_1, L and a constant is shown in figure 12. The maximum resonant λ decreases rapidly with respect to increases in $\Delta\psi = \psi_2 - \psi_1$,

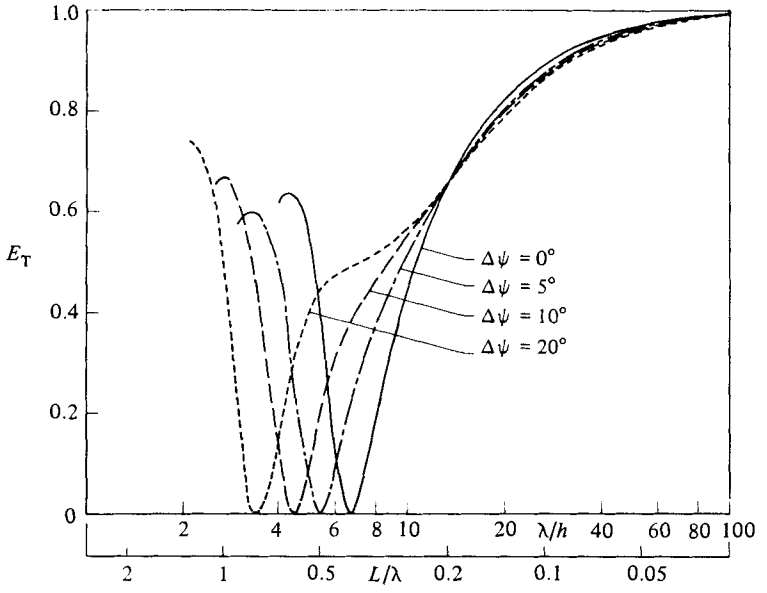

FIGURE 12. Energy-transmission response of wedge wavebreaker array near maximum resonant λ; $L/h = 2.667$, $a/h = 0.267$, $\delta/h = 0.08$ ($\psi_1 = 15.9°$). Values of $\Delta\psi$ shown.

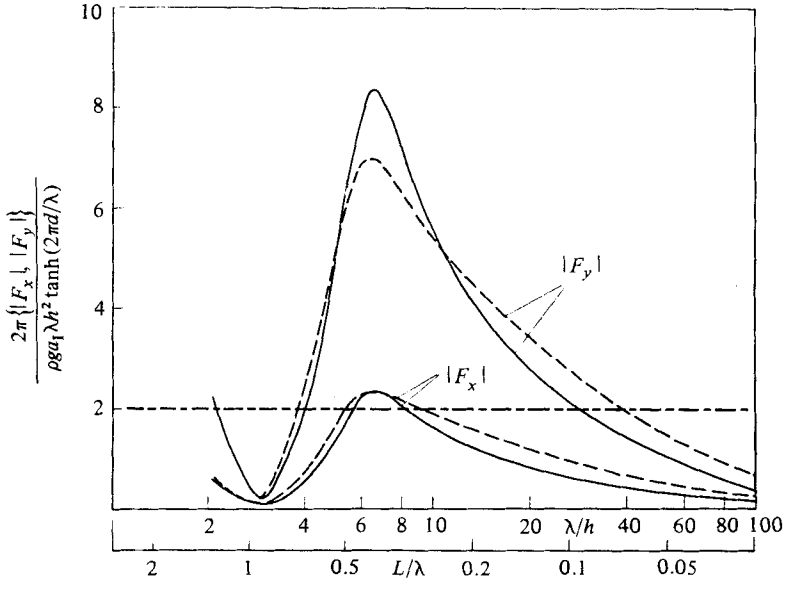

FIGURE 13. Magnitudes of oscillating forces in x- and y-directions; $L/h = 2.667$, $\delta/h = 0.08$; vertical lines indicate resonance: – – –, $a/h = 0.133$; ——, $a/h = 0.267$; — · —, F_x for solid wall.

indicating that the behaviour of the volume of water contained in the wedge of angle ψ_2 on the downstream side is strongly coupled with the incident wave at resonance. This somewhat counterintuitive result shows that the function of the gap in the breakwater behaviour is not restricted to allowing full transmission at high λ. It further suggests that possibility of 'tuning' the wavebreaker to resonance with the incident frequency through a variable-geometry control.

The magnitude of the oscillating forces on a half-wavebreaker as calculated from (20) are shown in figure 13 for $L/h = 2.667$. The large maxima near $L/\lambda \approx 0.40$ occurs because the wetted-surface profiles on each of the solid surfaces are out of phase as illustrated in figure 11 (*b*). In contrast, at the $L/\lambda = 0.9$ resonance the mean difference in the wetted-profile height is small (figure 11 *a*), leading to small forces and moments. It thus may be expected that further resonance at larger L/λ will lead to comparably small loads, so that the half-wave resonance is the only one which generates substantial forces. Note that for a solid-wall wavebreaker on $x = 0$ then $2\pi|F_x|/[\rho g a_I \lambda h^2 \tanh(2\pi d/\lambda)] = 2$.

5. Conclusions

We have investigated experimentally and theoretically the response of an array of convergent-channel wavebreakers to an incident single-mode wavetrain with $\lambda > 2h$. Each geometrical configuration studied was found to exhibit resonant behaviour ($E_T = 0$) at a finite sequence of incident wavelengths. The mechanism of resonance appears to be related to be the establishment of a nearly two-dimensional standing wave in each channel constriction, which in combination with an out-of-phase co-oscillation of fluid on the lee side of each channel wall generates strong upstream radiation and negligible transmission. In the present configuration with the wavebreaker fixed, the half-wavelength resonance produced sizable calculated transverse forces for each half-model (zero for each double wedge), and longitudinal forces comparable to those exerted on a solid-wall wavebreaker, while both force components were considerably reduced at higher-order resonances owing to cancellation effects. Some informal experiments conducted on a floating model, however, indicated that the $L/\lambda \sim 0.5$ resonance is not present in this configuration. Here a catamaran arrangement was used for lateral stability and buoyancy chambers were located at each wedge apex and stern to give longitudinal stability. It was noted that the $L/\lambda = O(1)$ resonance (with small forces) remained, but that, at $L/\lambda = O(0.5)$, the model followed the incident wave in a heaving motion with only a relatively small amplitude oscillation in pitch, and with large energy transmission and consequent small longitudinal forces.

The authors wish to acknowledge Mr H. E. Hunt and Mr A. K. Hamer who assisted with the collection of the experimental results.

REFERENCES

Buchwald, V. T. & Williams, N. V. 1975 Rectangular resonators on infinite and semi-infinite channels. *J. Fluid Mech.* **67**, 497–511.

Kinsler, L. E. & Frey, A. R. 1962 *Fundamentals of Acoustics*, 2nd edn. Wiley.

Mei, C. C. 1978 Numerical methods in water-wave diffraction and radiation. *Ann. Rev. Fluid Mech.* **10**, 393–416.

Morse, P. M. & Feshback, H. 1953 *Methods of Theoretical Physics, Part I*, chap. 7. McGraw-Hill.

Newman, J. N. 1976 The interaction of stationary bodies with regular waves. In *Proc. 11th Symp. on Naval Hydrodyn.* (ed. Bishop, Parkinson, Price), pp. 491–501. Mech. Engng Publ.

Srokosz, M. A. 1980 Some relations for bodies in a canal, with application to wave-power absorption. *J. Fluid Mech.* **99**, 145–162.

Transportable Breakwaters – A Survey of Concepts 1971 TR 727, *US Nav. Civ. Engng Lab., Port Hueneme, California.*

Ursell, F. 1951 Trapping modes in the theory of surface waves. *Proc. Camb. Phil. Soc.* **47**, 347–358.